Version of Record: https://www.sciencedirect.com/science/article/pii/S2214860423002324
Manuscript_8edf7331299f26504759260d992599fa

Impact of Controlled Prewetting on Part Formation in Binder Jet Additive Manufacturing

Colton G Inkley, Jacob Lawrence, Nathan B. Crane*

Brigham Young University, Provo, UT 84602, *nbcrane@byu.edu

ABSTRACT

Binder jetting is an additive manufacturing process that bonds powder through selectively depositing binder by inkjet printing. The part is then extracted and densified by sintering and/or infiltration. The process offers low costs and fast build rates, but properties can be poor due to residual porosity after sintering. The inkjet printing process may contribute to this residual porosity by creating large pores. The droplet kinetic energy ejects some powder particles from the bed and rearranges others. Particle ejection and rearrangement are theorized to create porous regions in binder-jetted parts. In this work, small amounts of moisture are added to the spread powder before printing and the impact on part formation, part properties, and printing parameters measured with varied droplet spacing, droplet velocity, and print frequency. Moisture is added by applying an atomized fluid mixture to the powder between layer spreading and binder printing. The fluid mixture partially evaporates but leaves a stable residue to increase cohesion and enhance imbibition. Moisture addition to the powder increases the range of droplet spacings for line formation while reducing particle ejection, powder rearrangement, and balling in layer and multilayer parts. Excessive moisture addition decreases the effective saturation of printed lines, but saturation in 3D parts is less impacted. Increased surface roughness in the first few layers of a print was also mitigated with prewetting. High-speed X-ray imaging verified prewetting reduction in particle ejection and rearrangement.

Keywords: binder jetting, surface roughness, prewetting, porosity, saturation, ink jet, synchrotron X-ray imaging

1 INTRODUCTION

Binder Jetting (BJ) is a powder-based Additive Manufacturing (AM) process that uses a binder deposited through inkjet printing to selectively bond powder. After printing binder, a new powder layer is deposited on top of the previously printed layer. The process repeats until a complete green part is formed. [1] The powder is typically heated between layers to promote evaporation of the binder solvent which substantially reduces process sensitivity to the printing conditions [2]. To reach a fully bound state the green part must undergo a sintering or infiltration process—improving part strength and density [1, 3].

Compared to other powder-based AM processes, BJ has several benefits. Since BJ utilizes binder to hold powder together, the process can be accomplished with virtually any powdered material including metals [4], polymers [5], and ceramics [6]. Additionally, BJ does not require significant thermal cycling during printing making the machines faster and cheaper than other AM processes. Finally, the unbound powder surrounding the bound part acts as a support for any overhangs present on the part being printed. However, the green part may shrink and/or deform

during post-processing [7, 8]. While progress is being made in understanding sintering methods [9], printing parameters [3, 10], the powder/binder interaction [11, 12], and green part saturation [13, 14], there is still much to learn about the process. For example, Schlachter et al. showed that concentrated polymer solutions deviate from capillary infiltration models [15]. While simulations of droplets impacting powder are progressing [16, 17], the models are still unable to capture the full physics of wetting and particle rearrangement at relevant size and time scales that match experiments. For example, Fuchs, et al. have illustrated a promising simulation framework for binder jetting and other AM processes that includes powder motion, but the demonstrated model size is too small spatially to represent the full droplet depth interaction and much longer simulations would be required to account for the critical interactions between droplets in lines and prior layers [18].

Thus most BJ printing research focuses on understanding the binder printing parameters and their impact on either the green parts or the final parts. Past research [10, 19-21] has shown how varying printing parameters including droplet velocity, size, spacing, and frequency effect green part quality and effective levels of binder saturation. Prints of single lines show balling when droplet spacing is too large, droplet frequency is low, or droplet sizes are too small [19]. Successful line printing in stainless steel showed a time dependence of balling formation of approximately $\sqrt{t}$ suggesting that Washburn infiltration may dominate the imbibition process [19]. Tan also showed Washburn infiltration of inkjet droplets on polymer powder but nearly constant imbibition rates for millimeter-sized droplets. Droplet spacing has also been shown to have large effects on green part saturation [19]. However, the results from individual lines do not predict successful conditions for layer printing [20]. Prewetting has shown promise in mitigating the varying effects of printing conditions on green part quality and saturation levels of single lines [22].

Although BJ shows promise, limits in final part strength and density for many materials has been a barrier to industrial use [1]. Parts made using BJ frequently show porous regions within the printed layers [23, 24] while porosity as low as 1-2% can significantly reduce part properties such as toughness, fatigue, and ductility [25-27]. BJ parts have been sintered to >99% density in multiple materials—often with the help of sintering aids [28, 29] and/or liquid phase sintering [30, 31], but large pores are always difficult to eliminate. These pores likely originate from the printing process given observations of pore structures within and between layers [32-35]. The spread powder layers are typically compacted effectively. However, powder particle rearrangement and ejection—caused during the powder-binder interaction—may generate the large pores that persist through sintering [32, 36] and result in residual porosity. Recent work printing binder in just the outer shell of the part showed that this increased the sintered density though it is unclear whether the benefits is due to less disruption from printing or less binder residue in the part [37].

The limited experimental observations of droplet impact under BJ-type conditions have been done in very different materials (steel - [36, 38], polymer [39], and slurry-based ceramic [40]). The different pore sizes, wetting conditions, and bed cohesion have resulted in varying observations of imbibition rates. As noted, the results of line printing don't necessarily predict printing of other geometries [20]. There is a significant body of data on millimeter-scale droplets impacting powders for granulation applications [41-46]. The map of different regimes (engulfing, tunneling, cratering, spreading) for granule formation developed by Emady et al. [42] would suggest that BJ printing conditions previously studied occurs near the proposed boundary

between spreading and cratering [39], or the boundary between cratering and engulfing [19]. However, the regime map only considers a single droplet in dry media. The presence of prior moisture dramatically alters the absorption [45] and so the regime map applicability to binder jetting is unknown. Additionally, most studies utilize loosely packed powder beds which have much lower porosity than typical of BJ powder beds. The loose packing can have a significant impact on the droplet absorption rate and may contribute to differences between BJ and other absorption studies [47]. Additionally, a comparison of millimeter-scale and micron-scale (inkjet-printed) droplets showed a very different time dependence on imbibition rates at the different scales [39].

Prior research has utilized surface roughness as a measure of BJ part quality [48, 49]. This research focuses on the surface roughness of printed layers as it impacts final part quality and may relate to low-density regions between layers. Colton et al. [50] showed that within the first five layers of a part, surface roughness changes significantly. From the unbound powder bed to the first printed layer, surface roughness can increase up to 60%. When a new powder layer is spread over this rougher surface, large pores may form if the powder does not fully fill the crevices. The increased surface roughness is likely caused by powder ejection during printing and/or balling [20]. Fan [51] used moisture within a powder bed to mitigate the surface roughness of lines. The results showed that moisture reduces particle ejection and in turn surface roughness, but the methods either created instability in line formation or left residuals within final parts. Colton's [50] results also showed that the addition of moisture to the powder bed had a positive impact on surface roughness but results were mixed. Some tested moisture levels resulted in little to no effect while others improved roughness but drastically increased part dimensions (bleeding).

The purpose of this paper is to report the impact of adding small amounts of moisture to the powder bed surface on BJ part formation, surface roughness, effective saturation, and part dimensions. Small amounts of non-binding fluids (prewetting moisture) can be added to the bed before binder printing to increase powder bed cohesion and speed binder absorption. However, if too much moisture is added, then it will likely increase droplet spreading resulting in lower saturation values, larger dimensions, and weaker green parts. To understand this tradeoff, the saturation and part dimensions for varying levels of non-binding liquid added before printing are reported for single lines, layers (groups of connected lines) and multilayer parts. The application of small moisture levels will be referred to as *prewetting* throughout the remainder of this paper. Previous work applying atomized water to the bed showed promise in single line printing [22], but the printing quality was highly dependent on the amount of moisture added and evaporation of the water after deposition made process control difficult. This work introduces alternative fluids that improve process control.

The residual moisture in the powder bed may speed droplet imbibition, create a cohesive force that also reduces particle rearrangement, and potentially reduce binder impact forces. As the droplets impact the surface, they will begin to infiltrate under the pressure generated by the impacting droplet and capillary forces. The speed of infiltration will be determined by the effective hydraulic conductivity of the powder bed. In partially saturated porous media, increasing saturation of porous media has been shown to increase the hydraulic conductivity 3-5 orders of magnitude [52, 53]. This will speed imbibition by reducing dependence on capillary flow. Increased imbibition rates may reduce the peak pressure and thus the force of droplet impact on the powder bed. Powder bed moisture will also create cohesive forces in the bed [54,

55] that may reduce powder rearrangement. The interaction of these phenomena are complex and both hydraulic conductivity and powder bed cohesion are sensitive to the local saturation levels.

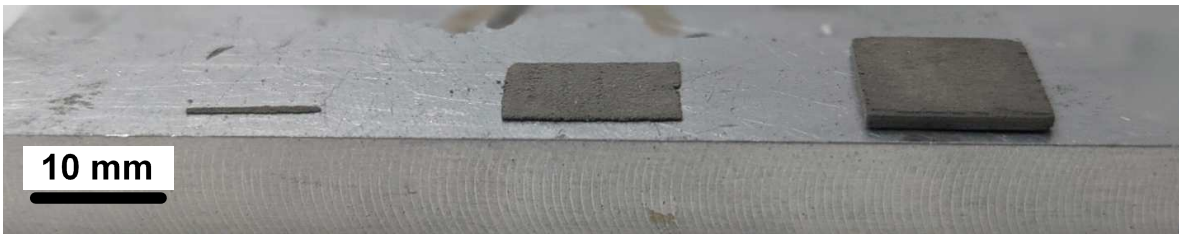

Figure 1: BJ parts used in this research. Left: BJ line, Middle: BJ Layer, Right: BJ Multi-layer.

2 METHODS AND MATERIALS

2.1 Key Process Parameters

2.1.1 Geometry

In commercial printing, a printhead with multiple nozzles traverses the powder bed. Typically, the nozzles are spaced far enough apart that they form separate lines of bound powder. The regions between nozzles are bound by additional passes with the same printhead or another printhead that follows behind the first. This is repeated with new layers of powder to create 3D parts. Thus, 3D geometry is typically formed from droplets that merge into lines. Additional lines are added to form layers which are stacked to form 3D geometry. This work will utilize a single printhead to study the formation of lines, layers, and multi-layers (Figure 1) with varied prewetting levels to measure the impact on each geometry. For this work, multi-layer parts are limited to three layers.

Line, layer, and multi-layer part formation can be altered by varying printing parameters such as droplet spacing, velocity, and frequency [19, 21]. Previous research [20] has shown that layers and multi-layers are printed most successfully at droplet spacings and line spacings close to 50 µm when printed with 46 ± 2µm diameter (~40 pl) droplets. However, these same droplet spacings do not form continuous lines in dry powder [19, 20]. These prior works are based on the same powder as used in this study.

2.1.2 Saturation

In BJ, saturation is defined as the fraction of void space between powder particles that is filled with binder during printing. Saturation is closely related to green part strength [10, 56, 57]. Typically, a target saturation level is set, and the droplet printing pattern is controlled to deposit the targeted amount of binder into the printed region. The target saturation (S_t) can be calculated using:

$$S_t = \frac{V_b}{(1-P_f)tA} \tag{1}$$

where V_b is the volume of deposited binder, P_f is the packing fraction of the packed powder material, t is the thickness of the layer, and A is the area where binder is deposited. Target saturation assumes that once deposited, binder will stay in place to define part geometry. However, binder often flows beyond these dimensions while volatile solvents in the binder evaporate. The actual saturation achieved in the part will vary spatially and over time. Methods have not been developed to measure the actual saturation levels in the parts. Instead, the effective saturation (S) is calculated from the measured part mass (m_p) according to:

$$S = \frac{\frac{m_b}{\rho_b}}{\frac{m_p}{P_f \rho_p} * (1 - P_f)} \quad (2)$$

where m_b is binder mass, ρ_b is binder density, m_p is part mass, ρ_p is the true density of the powder bed density (ρ_{ss}= 7.98 g/cm^3) , and P_f is the powder bed packing fraction [2]. Effective saturation is measurable and will be referred to as saturation throughout this paper.

If the effective saturation is below the target saturation, then binder has flowed beyond the part boundaries and the part is larger than intended. This is commonly referred to as bleeding [20, 58]. Because part saturation ties directly to green part strength [10, 59], the largest possible saturation without bleeding is typically preferred. Drying between layers keeps effective saturation levels close to the target saturation over a wide range of print saturation levels [2].

Prior research has sought to understand the effects of saturation. The first physics-based predictive model for saturation relied on capillary pressure measurements and cylindrical pore assumptions [13]. Predictions did not consistently match the effective saturation of lines, layers, or multi-layers, but provided an estimate. The deviations may be due to neglecting process parameters (droplet velocity, spacing, volume, and frequency) which have been shown to be significant [19, 21].

2.2 Printing Methods

To understand the effects of prewetting on printed lines, layers, and multi-layers, tests were conducted using varied droplet velocity, frequency, and spacing. The quantity of prewetting moisture and printed geometry were also varied. All inkjet printing was performed using a 30-micron orifice MJ-ABP-01 MicroFab piezo-electric inkjet nozzle. This is a single nozzle drop-on-demand printhead that is well-adapted for research. Droplet velocity was varied between 5 m/s and 7.5 m/s. Droplet velocity and volume were measured for each print condition as described below.

Prior work has shown that line formation is impacted both by the time between droplets (droplet frequency) and the distance between adjacent droplets [19]. For these tests, two frequencies of droplet printing were used: 1000Hz and 500Hz. Droplet frequency and droplet spacing are linked by the traverse speed of the nozzle. If frequency is held constant and droplet spacing changed, traverse speed must also change and vice versa. Specific droplet spacings were printed under two droplet frequency conditions to observe how altering the nozzle traverse speed/printing frequency altered printing results.

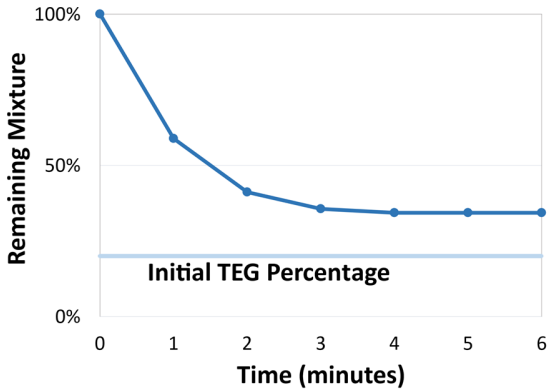

Figure 2: Evaporation of the 4:1 water/tri-ethylene glycol mixture. The percentage of tri-ethylene glycol remaining after the evaporation period is 34% of the initial mixture.

In prewetted powder beds, the spread powder layers were misted with a 4:1 volume mixture of water and tri-ethylene glycol before the binder was printed. Due to the high boiling point of tri-ethylene glycol (286.5 °C), a stable residue is left in the powder that is 34% of the initial deposited mass at room temperature as seen in Figure 2.

The stable residual level of the mixture provides for better experimental repeatability, but to assure that the parts reached the stable residual content consistently, there was a five-minute delay between misting and printing to allow for the fluid to reach the stable equilibrium level. All reported moisture levels are based on the estimated residual weight gain after the evaporation plateaued. For production, a more volatile liquid or an elevated bed temperature could be used to speed the evaporation process if desired. The prewetting would dilute the binder, but because it is not included in the effective saturation calculations, the saturation remains an effective comparison of binder content per unit volume of the printed geometries.

Lines were printed at varying droplet spacings with various levels of added moisture (0 (dry), 0.016, 0.039, 0.079, and 0.20 mg/cm^2). The prewetting level was measured by measuring the weight gain of a thin layer of powder after exposure to the atomizer under the test conditions and normalizing by the area of the bed. The uniformity of the atomization process over was evaluated by comparing weight gain of smaller (25 mm x 25 mm)beds located in different regions of the bed and found to be within 10% [22]. The effective saturation and dimensions of the lines were measured to identify moisture levels that were most likely to improve printing without causing low resolution and low strength due to excessive bleeding.

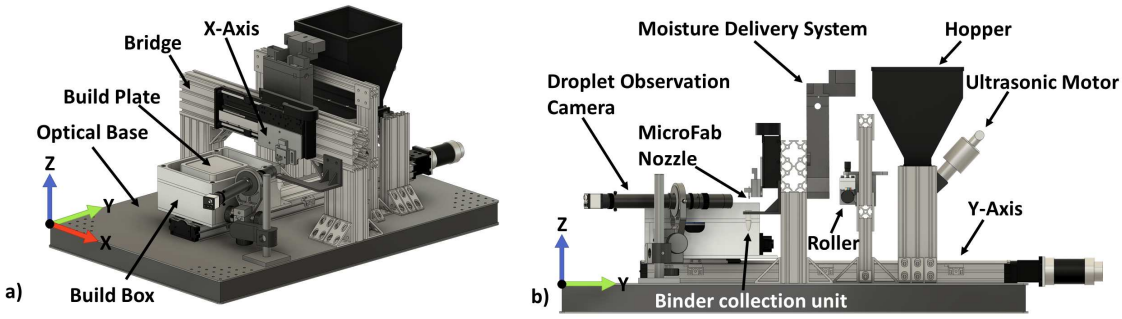

Figure 3: Custom binder jetting equipment used for this work. a) Isometric view of the printer. b) Side view of the printer. The y-axis moves the build area underneath the hopper which deposits powder. The y-axis then brings the build area forward where a roller packs and levels the powder. The x-axis and y-axis work in conjunction to move the nozzle to print binder in the desired areas. This process was repeated for multi-layer parts.

Prewetting partially pre-saturates the powder bed. Pre-saturation level of the powder after evaporation were estimated for the tri-ethylene mixture for each of the prewetting moisture conditions using a variation of Eqn (2). The prewetting penetration depth was estimated from the depth of lines printed into the pre-wetted powder. A sessile droplet would generally penetrate at least as deep as the interconnected fluid network created by prewetting. The kinetic energy of the droplets will generally push the binder beyond the sessile droplet limit. Thus, this approach probably overestimates the prewetting depth, and the resulting saturation estimate is a lower bound.

2.2.1 BJ Test Platform

A custom BJ printer (Figure 3) was used for testing in this research. Printer capabilities include powder deposition and spreading as well as single and multi-layer printing. The build-box—held by the y-axis—was designed to hold powder for part fabrication. The x-axis was mounted to the bridge and moved the MicroFab piezo-electric printhead used for binder delivery. The z-axis was built into the build-box and moved the build plate up and down when printing multi-layer parts. The printer enabled automated droplet observation, powder deposition, moisture application (prewetting), and printing. Additional system details are available in [60].

Powder is deposited from a hopper with an ultrasonic motor and then rolled with a counter rotating roller as the y-axis moves the build box under each section. Ten base layers are rolled before part fabrication. The packing fraction was calculated using the plug method, where a hollow cylinder with a known inner diameter is placed into a packed powder bed, then the plug of powder removed and weighed [24]. The packing fraction measured for these tests was 55%.

The water/triethylene glycol mixture was applied to the spread powder by atomizing it with a piezo-electric atomizer (16 μm diameter holes at 150 μm pitch) run at 113KHz as described in [22]. The use of a duty cycle allowed for fine control over the quantity of the atomized fluid. Two atomizers were fitted into the conduit and tuned using a PWM signal to achieve uniform distribution across the bed [22]. Once the moisture delivery system was activated, the y-axis moved the build box at a constant velocity under the conduit. After printing, the moisture evaporates until it reaches equilibrium as seen in Figure 2.

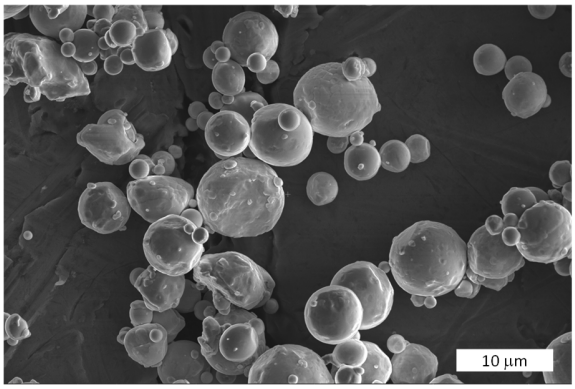

Figure 4 SEM image of stainless steel 316L powder used in the experiments

Inkjet droplets were observed using LED strobe lighting to capture jetted droplets at varying positions during their descent. These captured observations were then used to calculate the droplet velocity. Droplet volume was measured by jetting into a container at a known frequency for three minutes. The container and binder were weighed using an OHAUS Adventurer Analytical scale with a ±0.1 mg resolution. Droplet volume was calculated from the density of the binder (1.04 g/cm^3) and the number of droplets printed. The size of the droplet exiting the nozzle was held constant throughout testing and was 46 ± 2 µm across the range of droplet velocities tested. A small negative pressure was applied through a MicroFab pneumatic console. Pressure was adjusted to achieve stable operation at the target droplet velocity.

2.3 Part Fabrication

All parts were fabricated using ExOne's 316L stainless steel powder with an average particle size of 10 µm [19, 20]. The material is gas atomized and generally spherical as seen in Figure 4. ExOne's BA005 Aqueous Binder was used in all printing. The binder manufacturer reports the binder properties as ($\rho = 1.11\ g/cm^3$, $\mu = 5.8\ cP$, $\gamma = 35\ dyne/cm$). Lines were printed according to the parameters listed in Table 1. A range of droplet spacings was printed for each parameter set, resulting in a total of 60 data sets. Six lines of each droplet spacing were printed with a spacing of 6 mm between lines to ensure no interaction between them. When moisture was applied to powder beds, five minutes elapsed between moisture application and ink jet printing to ensure stable moisture levels during testing.

Table 1: Printing parameters tested in line printing.

Droplet Velocity (m/s)	Frequency (Hz)	Droplet Spacing (µm)	Moisture conditions (mg/cm^2)
5	1000	15, 20, 25, 35, 45, 55	Dry, 0.016, 0.039, 0.079, and 0.20
5	500	15, 20, 25, 35, 45, 55	Dry, 0.079
7.5	1000	15, 20, 25, 35, 45, 55	Dry, 0.016, and 0.079

Single layer and multi-layer parts were printed by depositing 85 adjacent lines according to the parameters listed in Table 2. Droplet spacing of 50 µm and 60 µm were printed for each parameter set, resulting in a total of 30 data sets. Five parts of each set were printed. The spacing between lines was equal to the droplet spacing and a layer height of 35 µm was used in the multi-layer parts. Two-layer parts were started on the second layer of the three-layer part build. Thus, the top surface of all parts was visible at the top of the build plate. Single layer parts were printed separately.

Table 2: Parameter sets used in multi-layer printing.

Droplet Velocity (m/s)	Frequency (Hz)	Droplet/Line Spacing (µm)	Moisture conditions (mg/cm^2)	Number of Layers
5	1000	50, 60	Dry, 0.016, 0.079	1, 2, 3
5	500	50, 60	Dry, 0.016, 0.079	1
7.5	1000	50, 60	Dry, 0.016, 0.079	1

After printing, the powder bed was placed in a Hotentogler Binder Series ED Avantgarde oven at 180℃ for at least 30 minutes to cure the binder. Once the samples had cooled, a two-pronged fork was used to extract samples by putting the two prongs into the powder bed and lifting the samples out. Samples were imaged using a VHX-7000 Keyence digital microscope. Both 2-D and 3-D images were taken both before and after extraction from the powder bed. For lines, widths and depths were recorded. For layer and multi-layer parts, widths, lengths, and depths were recorded. Surface roughness measurements were taken on the top surface of layer and multilayer parts using an optical 3-D profilometer (Zeta instruments, Zeta 20). Surface topography was measured in optical profiling mode using focus variation at 20x magnification with a 0.1 µm z-resolution.

After imaging, parts were weighed using an OHAUS Adventurer Analytical scale with 0.1 mg resolution. The total weight of all the parts in a single data set was obtained and the average weight calculated. The effective saturation was then calculated using the average weight of all samples of a type, a binder mass calculated from the droplet volume, and the packing fraction of the powder bed.

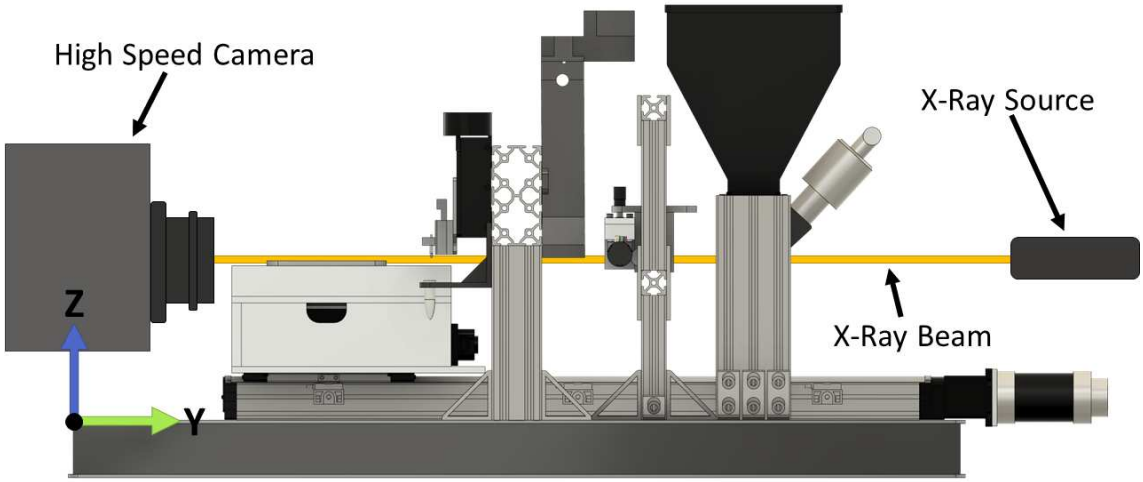

Figure 5: Setup for x-ray imaging at APS. The x-ray beam window was approximately 2 mm x 2 mm. For testing at APS, the hopper was removed, and a hand prepared x-ray transparent build box of glassy carbon was mounted in place of the build area. For the x-ray to penetrate through stainless steel powder the build box was designed to reduce the material thickness to less than

To estimate uncertainty in the measurements, the variation for saturation values was obtained for both dry and the 0.016 mg/cm^2 moisture conditions for lines, layer, and multi-layer parts. For lines, standard deviation values were recorded by printing 20 lines at each droplet spacing and finding the average saturation value for each set of four lines. Layer and multi-layer standard deviations were recorded by printing three to five samples and comparing the saturation values of each sample.

2.4 High-Speed X-ray Imaging

The printer setup was also used to conduct experiments using a high-speed synchrotron x-ray imaging system at the Advanced Photon Source (APS) at Argonne National Laboratories Beam 32-ID-B. Additional details about the setup and conditions are reported in [61]. The printer was positioned between the x-ray beam and image processing unit (Figure 5). High-speed x-ray images of the BJ process were captured. The same 316L powder, ExOne binder and printing procedures were used. To enable X-ray transmission through the sample, the hopper was removed, and an x-ray transparent build box of glassy carbon with a ~450 μm wide slot was mounted in place of the build box. The slot was filled with powder and leveled with a razor blade. Up to five adjacent lines were printed in the box to observe interactions between lines. Moisture was applied to a subset of the beds using the 0.016 mg/cm^2 prewetting level and allowed to equilibrate before testing.

Two printing directions were used. Parts were primarily printed by moving the printhead in the x-direction with the x-ray beam oriented along the y-axis. This setup captured line printing as it traverses across the point of view from left to right. Some parts were printed by moving the powder bed on the printer y-axis relative to a stationary printhead. In y-axis printing, the line is parallel to the X-ray beam so that the width and depth of the printed line are both observable. Because most of the build-boxes were not prepared using a roller, the results, may deviate from rolled powder beds typically used. A few tests were conducted using rolled powder for comparison. For rolled powder tests, the powder was rolled on a small elevated platform. After

rolling, a razor blade was used to reduce the width of the powder bed size to allow x-ray transmission.

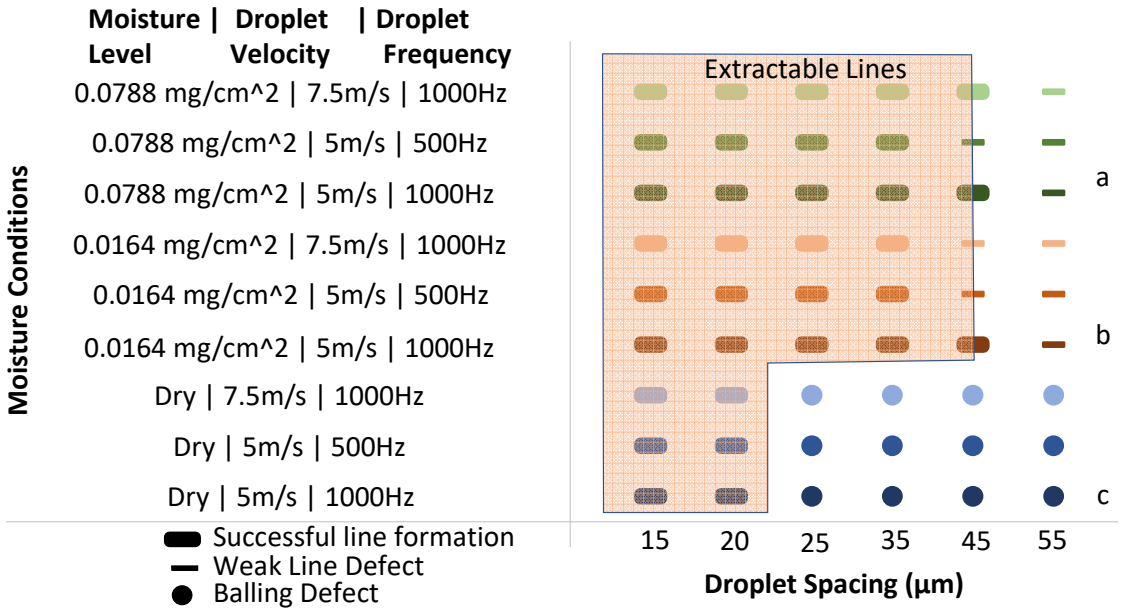

Figure 6: Line formation outcomes as a function of printing conditions (droplet spacing, print frequency, droplet velocity). Prewetting not only increases the parameter set resulting in successful line formation, but also eliminates balling typically seen in lines. All pictures correspond to the 5m/s | 1000Hz lines.

3 RESULTS AND DISCUSSION

Results are organized by the type of printed geometry: lines, layers and multi-layers. Lines were used to measure the results of prewetting on line formation, dimensions, and saturation levels. From these results, the most promising moisture levels were selected for evaluating single layer and multilayer parts. Single Layer and multi-layer parts are used to compare phenomena observed in line printing to single and multi-layer parts for both dry and prewetted powders.

3.1 Lines

Although line printing results do not predict the range of printing parameters that make successful parts in layers and multi-layers as has been shown previously [20], they are useful in quickly observing changes in powder/binder interaction and other phenomenon such as balling. For this research, individual lines were printed to narrow the range of prewetting conditions to study in layer and multilayer geometries. Saturation, part dimensions, and print failure modes were analyzed for each level of prewetting.

3.1.1 Line Formation

Figure 6 summarizes the success of line formation as a function of the printing parameters. The lines printed into dry powder are compared to those prewetted with 0.0164 mg/cm^2 and 0.0788 mg/cm^2 of the water/triethylene glycol mixture. Lines printed into dry powder could not be extracted at droplet spacings larger than 20 µm due to onset of balling as seen in Figure 7. In contrast, all lines treated with prewetting had lines successfully extract at droplet spacings of 35

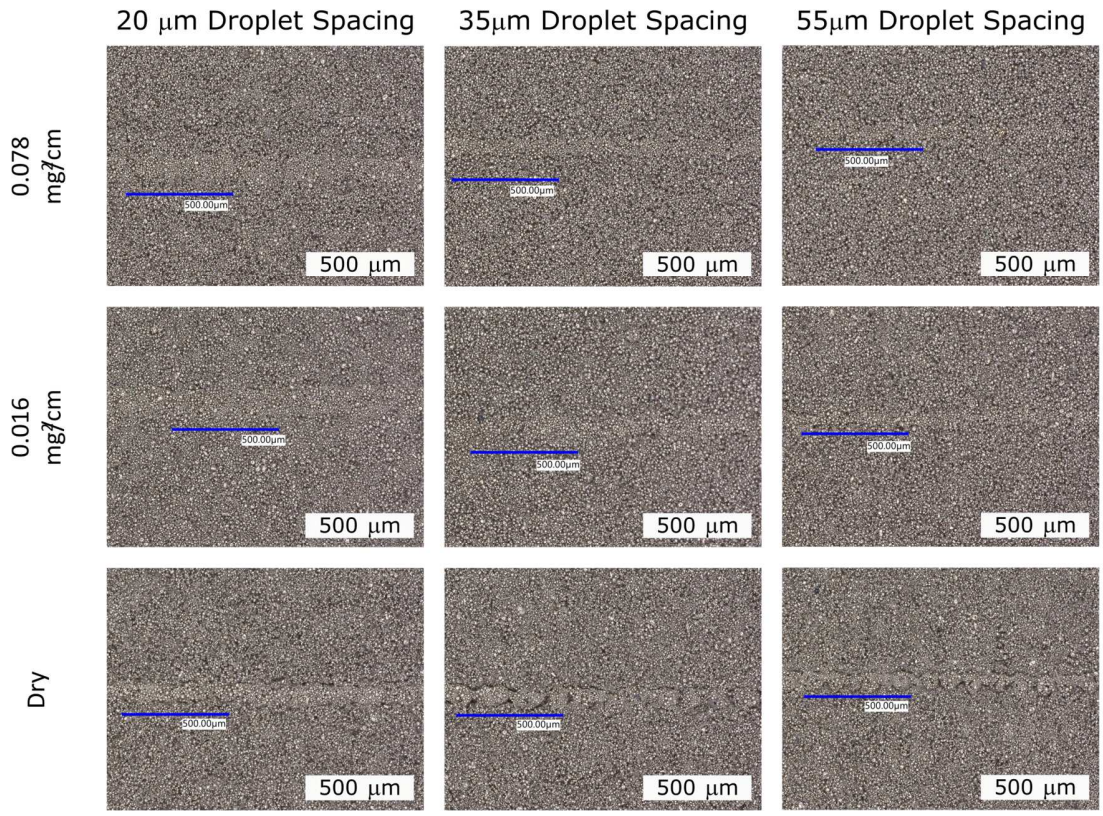

Figure 7: Optical images of the printed lines show that moisture addition mitigates particle rearrangement as printed lines become difficult to see in the prewetted cases. Pictures on the bottom correspond to lines on the graph, matching the colored shapes and the number indicating droplet spacing. All pictures correspond to the 5m/s | 1000Hz lines. Letters on the right correspond to labels in Figure 6

μm and in many cases 45 μm. Beyond this point, the lines appeared continuous but were too weak to be extracted. Negligible differences were observed between droplet velocity of 5 m/s and 7.5 m/s and printing frequency of 500 and 1000 Hz.

Balling occurs when the droplets are too far apart and revert to the shape that minimizes surface energy–a sphere. In balling, the line breaks into a series of spherical primitives. Lines printed onto prewetted powder beds did not experience balling at any tested droplet spacing (Figure 6). The suppression of balling by prewetting could be due to formation of a liquid network between powder particles which is speeding infiltration of the droplet into the powder and/or increasing cohesion of the powder to reduce powder rearrangement required for ball formation.

The prewetting is not only mitigating balling, but also eliminating particle rearrangement caused by binder impacting the powder. The images in Figure 7 show that the lines printed in dry powder have clearly visible boundaries. The boundaries are caused by powder motion during printing. However, it is difficult to visually differentiate the bound region of powder from the unbound region in the prewetted powder due to reduced rearrangement. If prewetting reduces particle rearrangement, it has the potential to reduce or eliminate defects created during printing.

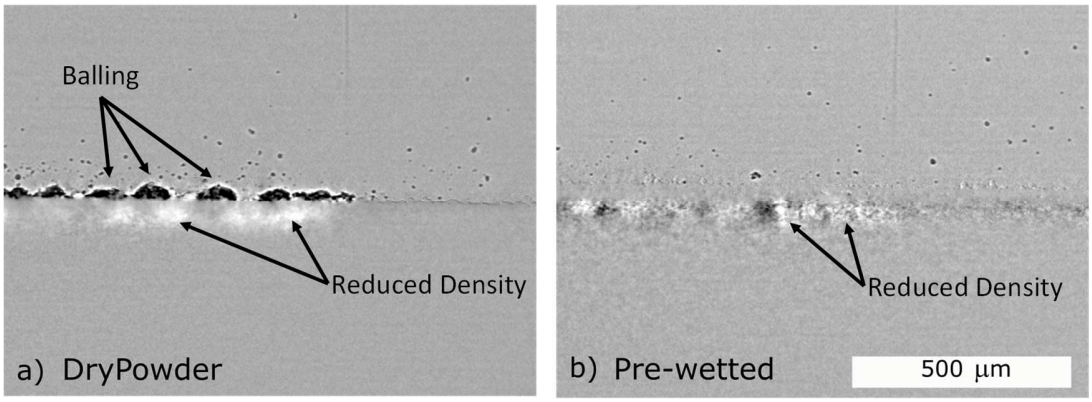

Figure 8: High-speed x-ray images of BJ process on loose powder leveled with a razor blade. The image before printing was subtracted so that increases in density show as brightness decreases and regions with decreased density are brighter. a) Line printed into dry powder. Balling can be seen starting at the left of the image. b) line printed into prewetted powder (0.016 mg/cm^2). Balling is eliminated due to moisture within the powder though some spatial variation in density was introduced. Both lines were printed using the same printing parameters (Droplet spacing: 50 µm, Droplet Velocity: 7.5 m/s). X-ray framerate was ~50000 frames per second with an exposure time of 19 µs. The full video is available as a supplementary document (LoosePowder.mp4)

X-ray imaging experiments conducted at APS confirm the elimination of balling with prewetting. The initial image before printing was subtracted from later frames to highlight changes in the X-ray absorption due to printing. Reduced absorption (lower density) appears brighter. Figure 8 shows a comparison of lines printed using a parameter set which is known to cause balling in dry powders (droplet size: ~45µm, droplet velocity: ~7.5 m/s, droplet spacing: 50 µm). The entire video sequence is available in the supplementary information (LoosePowder.mp4) Balling is clearly visible in the dry powder as dark regions of increased density while the prewetted powder eliminates balling and reduces other particle rearrangement as seen by smaller variation in brightness. Both cases show ejected particles above the bed of loose powder, but prewetting reduced the number of ejected particles by 25%.

The benefits of prewetting on reducing powder rearrangement and particle ejection were even larger in imaging of rolled powder beds. Figure 9 shows a comparison of high-speed X-ray imaging of lines printed into 316 SS powder. The video is available in the supplementary information (RolledPowder.mp4). In the image of dry powder printing, particle rearrangement can clearly be seen with dark regions that have densified during printing and brighter regions where powder has been removed. Additionally, particle ejection is observed above the powder bed. However, in the prewetted powder, the number of ejected particles was reduced by 65% by prewetting, and no bright spots are visible that would indicate pore formation. These tests in rolled powder should closely approximate realistic printing conditions. Prewetting strongly reduces balling and powder rearrangement in line printing.

While recent stroboscopic imaging of larger droplets (95 µm) at slower speeds (4m/s) revealed distinct droplet spreading over a period of more than 300 µs in when printing on a polymer powder [39], there was no observable droplet spreading in the X-ray images. The droplet completely disappeared beneath the surface of the powder in a single frame (20 µs). The

smaller droplets and higher velocity in the present study both would reduce the infiltration time, but do not fully explain the differences in infiltration characteristics.

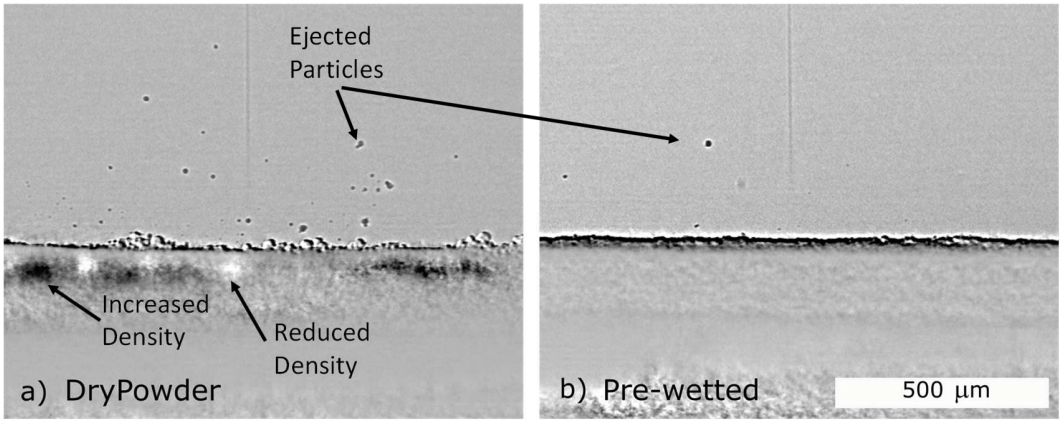

Figure 9: Comparison of powder bed density changes and powder ejection due to line printing in rolled powder. Original x-ray images were post processed by subtracting off a non-changing frame to highlight changes in brightness. Increases in density show as brightness decreases and regions with decreased density are brighter. a) Line being printed into a dry powder bed; significant particle ejection can be seen. Bright and dark regions under the printing surface reveal particle rearrangement within the bed. b) Line being printed into prewetted powder; only a few ejected particles can be seen. Much less particle rearrangement is present. Lines were printed using the same printing parameters (Droplet spacing: 50 µm, Droplet Velocity: 7.5 m/s). X-ray framerate was ~50000 frames per second with an exposure time of 19 µs. The full video is available as a supplementary document (RolledPowder.mp4)

3.1.2 Line Saturation

Saturation values in printed lines (Figure 10) generally decrease with increasing droplet spacing and increasing moisture content. The decrease in effective line saturation at high levels of pre-printing moisture is evidence of a percolating moisture network created by the prewetting. This percolating fluid network facilitates binder spreading in the powder bed due to both the kinetic energy of arriving droplets and capillary flows in the bed. Because the same binder spreads over a larger region, line dimensions increase while strength decreases. For lines printed in pre-moistened powder, saturation values generally decrease as droplet spacing increases. However, the lowest and greatest recorded saturation values for each prewetting level stay within 10% of one another as the droplet spacing increases 3x.

The difference between saturation in the 0.0388 and 0.0788 mg/cm^2 moisture levels is negligible, whereas the extreme values (0.0164 mg/cm^2 and 0.1997 mg/cm^2) deviate significantly. These results suggest that there may be different dominant phenomena in the different prewetting levels. While prewetting has reduced saturation, there appears to be a broad range of prewetting values that achieve similar printing outcomes which is promising for development of a robust printing process with prewetting. Saturation changes due to velocity (7.5 m/s, 5 m/s) and droplet frequency (500 Hz, 1000 Hz) were generally varied by less than one standard deviation (Figure S1 and S2).

3.1.3 Line Aspect Ratio

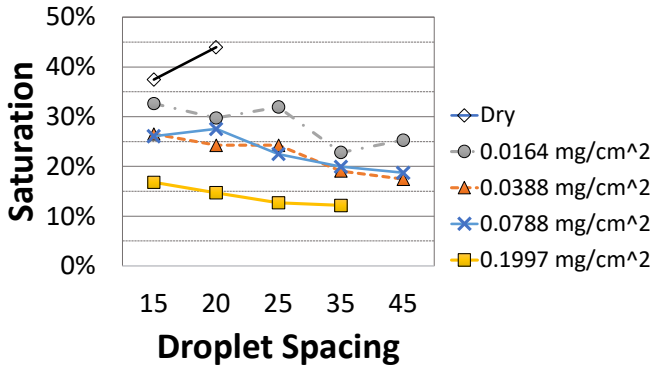

Figure 10: Saturation values for lines under different prewetting conditions. Values not represented indicate a line that did not successfully form. Representative standard deviations in measured saturation for dry and 0.0164 mg/cm^2 were 1-2% and 0-4%, depending on droplet spacing, respectively. There was a single 55 μm droplet spacing line that was successful for the 0.1997 mg/cm^2 moisture condition that was not included in this graph due to its singularity.

The aspect ratio of printed lines is indicative of the relative rates of binder migration in the horizontal and vertical direction. As seen in Figure 11, droplets printed in dry powder, had an aspect ratio (width/depth) of 1-1.5 indicating relatively similar rates of spreading in both directions. However, the pre-moistened lines have significantly higher aspect ratios. The three lowest prewetting values have an aspect ratio of approximately two while the largest prewetting level generates lines with an aspect ratio over three. This increased aspect ratio indicates that the droplets spread horizontally more easily than vertically.

Partial saturation of a porous media is known to increase hydraulic conductivity by orders of magnitude relative to dry powders [53, 62, 63]. If the added moisture is non-uniform through the depth, this would create a high conductivity layer at the top that could promote horizontal spreading. As the binders penetrate deeper (as for closer droplet spacings) the droplets will reach progressively drier powder and the difference between the horizontal spreading rates and in-depth absorption will increase further. Note that the 15 μm droplet spacing produces the largest aspect ratio under all wetting conditions. With increased droplet spacing, the aspect ratio generally decreases though the different prewetting levels produced different effects. The highest prewetting produces aspect ratio > 3 under all droplet spacings while the intermediate prewetting levels had aspect ratio near 2 across most test regions.

Aspect ratios significantly greater than one are expected to reduce the planar resolution of the printing process because a positive feature cannot be smaller than a single line width. However, an aspect ratio of two may not significantly impact the printing capabilities when printing multi-layer parts as the previously printed layers will likely absorb binder and reduce the horizontal spreading of the new line beyond the part dimensions. Additionally, the repeated misting of multi-layer parts after each spread layer may also create a more uniform moisture profile through the part thickness than observed in lines and single layers to reduce the aspect ratio of individual lines.

All printed lines penetrated more than one layer deep into the powder (Figures S3 and S4). Penetration through an entire layer is critical to bind multiple layers together. The depth penetration may also be reduced when printing adjacent lines to form layers.

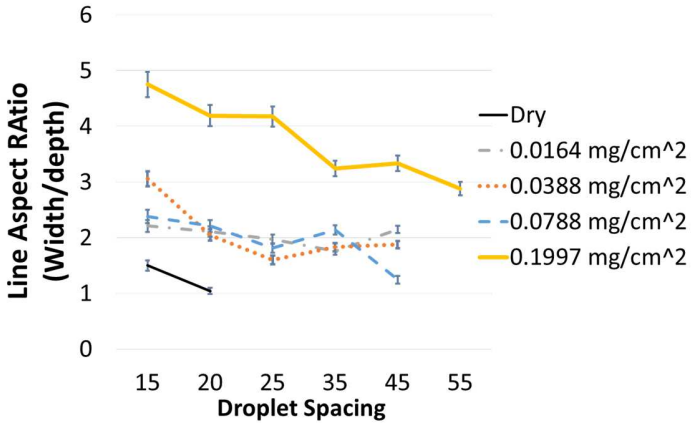

Figure 11: Aspect Ratio of printed lines (width/depth). Values not represented indicate a line that did not successfully form. In dry lines the aspect ratio of width to depth stays close to one, but moisture increases the ratio dramatically. Adding moisture increases the width more than the depth, which is evident in the rise in aspect ratio. Prewetting facilitates a horizontal spread of the binder throughout the powder bed and tends to limit binder spreading below a certain

3.1.4 Insights from Prewetting Impact on Line Printing

In ideal prewetting, a small amount of moisture would be deposited uniformly through the layer below the percolation threshold. If prewetting saturation exceeds the percolation threshold, the binder will spread readily through the bed through both capillary flow and diffusion resulting in lower saturation, weaker parts, and decreased print resolution. Unfortunately, the percolation threshold for these rolled powder beds is unknown and no methods are available for measuring the local saturation achieved by the prewetting process.

It is also unlikely that the moisture in the powder bed is distributed uniformly. The atomized droplets generating by vibrating the plate with 16 μm holes are likely too large to penetrate far into the powder bed as discrete droplets given that the pore path in a packed powder bed would be tortuous and the pores small. Thus, they are likely deposited on the surface and then wick into the powder bed under capillary action—creating a percolating pore network through the wetted regions. Thus, misting alone may be unable to create anything but a percolating threshold. However, the subsequent evaporation of >60% of the fluid may be sufficient to create a non-percolating moisture network when depositing low levels of moisture.

While measuring the saturation in the surface layer is infeasible, saturation can be estimated by assuming that the saturation is uniform through the surface to a depth of the lines printed at that moisture level. Table 3 summarizes the estimated average saturation values after the initial evaporation. These saturation levels are low enough that they are likely to be below the percolation threshold. While the percolation threshold varies widely in some reports [64, 65], careful experimentation concluded that in packed beds of spheres, it is generally in the range of 6-10% saturation for a wide range of fluids and particles [66].

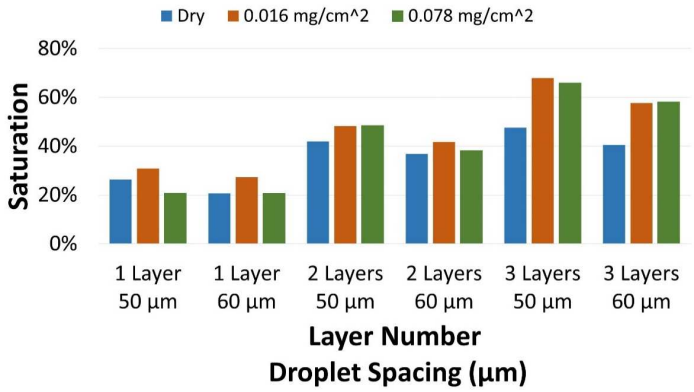

Figure 12: Part Saturation variation with number of layers, droplet spacing and prewetting moisture level. Standard deviation of saturation for both layers and multilayers printed at 50 µm droplet spacings into dry powder were 0.57% and 2.03% respectively. Standard deviation values for both layers and multilayers printed at 50 µm droplet spacings with 0.0164 mg/cm^2 prewetting fluid were 0.88% and 3.74% respectively.

Table 3: Estimated Average Saturation Levels Due to Prewetting

Prewetting Level (mg/cm^2)	Average Line Depth (µm)	Estimated Avg Saturation (%)
0.016	111	0.34
0.038	118	0.71
0.078	131	1.3
0.199	120	3.6

3.2 Layers and Multi-Layers

The data from the line tests were used to select two moisture levels for layer and multi-layer part printing. The 0.1997 mg/cm^2 prewetting condition shows saturation levels which would result in weaker/undeveloped parts, indicate a poor candidate for further testing. The three lower prewetting moisture conditions had similar aspect ratios (Figure 11) indicating that none was clearly superior in printing better geometry. However, the 0.0164 mg/cm^2 moisture condition is promising because saturation values are consistently higher than the other moisture conditions. Two pre-moisture conditions were desired for further testing and the 0.0788 mg/cm^2 moisture condition resulted in slightly superior saturation results over that of 0.0388 mg/cm^2 so it was also chosen as the second prewetting condition for layer printing.

Single layer and multi-layer prints were conducted to represent actual printing conditions during formation of 3D geometry. Although all the parameters laid out in Table 2 were tested, the droplet frequency or droplet spacing didn't provide significant variation in the layer data. Therefore, data on frequency and droplet velocity is reported in supplementary information.

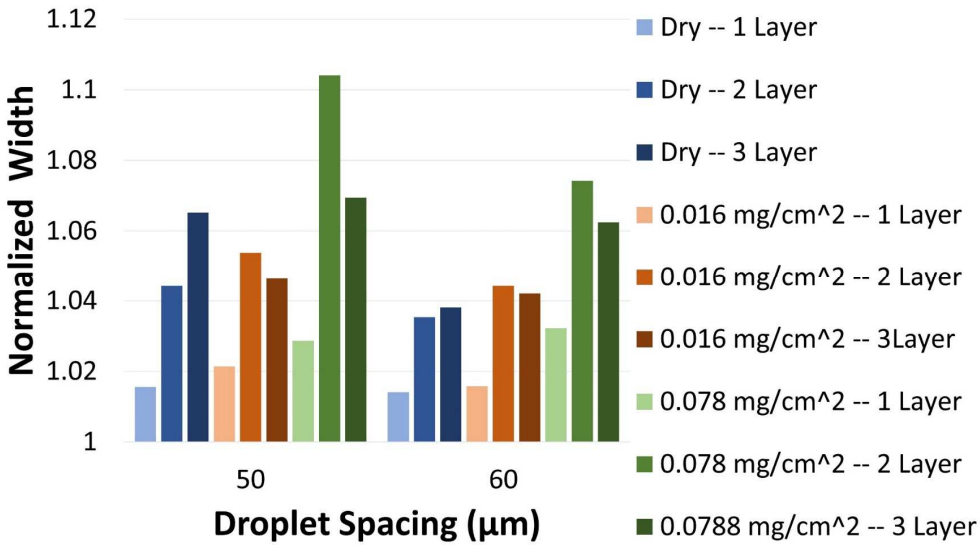

Figure 13: Normalized Width vs. Droplet Spacing for different numbers of printed layers. The widths were normalized by the distance between the center of the first and last lines to normalize for the different line spacings (line spacing = droplet spacing). Normalized width increases with larger pre-moisture conditions but decreases with droplet spacing. Part width increases with layers for dry powder, but interestingly in prewetted parts, the width decreases after the 3rd

3.2.1 Saturation

While both prewetting levels have similar saturation, prewetting of 0.0164 mg/cm^2 typically shows higher saturation results than 0.0788 mg/cm^2. Saturation values increase with increasing layer number as shown by Colton [20], but surprisingly, saturation values also increase with prewetting. This is opposite the trend observed when printing lines into prewetted powder. The difference in saturation between dry and prewetted powders increases with layer number at both moisture levels. This increase in saturation through prewetting is a potential benefit as it typically correlates with greater green part strength [10, 59]. While the saturation levels vary with the number of layers (one, two, or three) and the droplet/line spacing (50 µm, 60 µm), the prewetting levels did not substantially change the saturation in the two and three-layer samples. The low sensitivity of saturation to print parameters would be helpful in creating a robust process.

The increases in saturation with prewetting in multilayer parts is unexpected and may be related to evaporation of binder solvent. The delay between misting and printing was added to allow for stable evaporation of the prewetting fluid, but it also may be allowing for binder evaporation from the prior layer as well as prewetting. This evaporation of binder solvent during the delay would have similar impact as powder bed heating which has been shown to increase the effective saturation levels [2]. Thus, the increased saturation observed in prewetted parts may be at least partially due to the delay between layers rather than the prewetting itself.

However, in a production process, the benefit of increased saturation could also be obtained by adjusting the heating between layers.

The increase may also be due to defect mitigation in the prewetted powder observed in Figure 8 and Figure 9. The formula for effective saturation (Eqn 2) shows a connection between saturation and powder bed density can be made. For constant part mass and binder volume,

$$S \propto \frac{P_f}{1-P_f} \tag{3}$$

Thus, as the packing fraction (P_f) increases, so does saturation. A lower saturation in the dry parts could be caused by defects generated during printing that reduce the packing saturation. However, the saturation values are calculated based on the assumption of constant packing fraction, so conclusions cannot be drawn regarding the part level saturations from this data.

Droplet velocity and frequency had some effects on the resulting saturation of the first printed layer as discussed in the supplemental information seen in Figure S5 and S6. However, these impacts are much smaller than the difference between the first layer and second layer of a print. While they may be important in forming very fine features and in roughness of the bottom surface, drop velocity and frequency effects in the tested range studies will not be significant to the printing of most 3D parts.

3.2.2 Dimensions

The variation in part dimensions with saturation gives insight into whether binder bled beyond the desired geometry. In-process heating is typically used to reduce the impact of saturation levels on part accuracy [2]. Because this work did not use any in-process heating to promote binder evaporation, the effective saturation values are more sensitive to the printing conditions. The width (perpendicular to line printing direction) of the printed layers can indicate bleeding levels. Figure 13 shows that prewetting increases the width of single layer parts. Width increases further with the addition of a 2nd layer in all combinations of droplet spacing and prewetting states. However, the magnitude of the increase varies. At 0.0164 mg/mm^2, the width difference between the wet and dry powder is generally negligible (<0.5%).

These dimensional measurements show that the assumption of constant geometry with different prewetting levels does not fully hold. While changes in geometry due to moisture addition are undesirable, this effect could be mitigated through process parameter adjustments or in-process heating to evaporate binder solvent. After the first layer, the differences in dimensions between the prewetted and dry powder decreases and is even eliminated under some conditions. Thus, dimensional errors are not expected to be a significant issue under tested prewetting conditions.

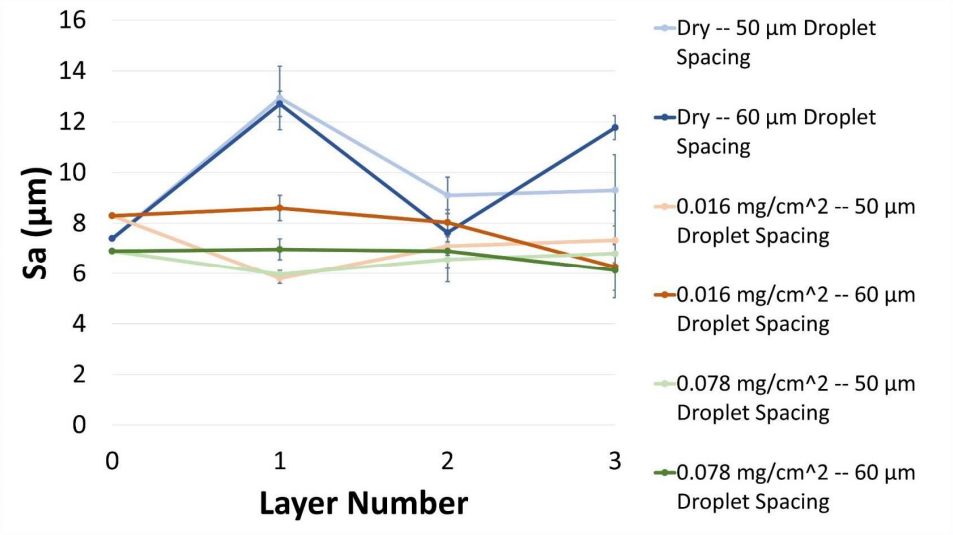

Figure 14: The change in Sa as layers increase. Data points are an average of three measurements. Data points located at a layer number of '0' indicate the surface roughness of the powder bed before part printing. Prewetting of the powder not only reduces drastic changes in Sa with increasing layers seen in the dry powder, but also keeps Sa values close to or below Sa values of the pre-printed powder. Error bars represent one standard deviation.

The dimensional changes do not explain the saturation differences in prewetted parts because the larger dimensions of the prewetted parts would tend to decrease the saturation, but these may be offset by smaller printed depth. Parts in prewetted powder have reduced width of the three-layer parts compared to the two-layer parts while the width of the parts printed in dry powder continues to increase with additional layers. This may be due to a decrease in imbibition rates in the vertical and horizontal directions. In the multi-layer parts, each layer is misted so that the through thickness uniformity of the imbibition rates may increase with additional layers. Additionally, the prior layers are wetted with binder which can also reduce spreading. This may explain the improved accuracy of the multi-layer parts. Even high levels of moisture addition may approach the target dimensions when printing multilayer parts. Future testing of more layers may provide further insights into these observations. In future work, multi-layer parts could be either partly sintered or infiltrated, sectioned, and analyzed to obtain a better understanding of whether prewetting is influencing void formation within the first few layers of a print.

3.2.3 Surface Roughness

Colton et al. [20] showed that surface roughness (Sa) increases above that of the undisturbed powder bed over the first 2-3 layers, but then decreases down to levels comparable to the undisturbed powder bed by layer 5. Colton speculated that the increased Sa was caused by balling during the formation of a layer. The increased surface roughness within these first few layers could be the cause of some BJ defects due to difficulty of filling the crevices with powder during subsequent layer spreading operations. Surface roughness itself is also an important quality metric in many components.

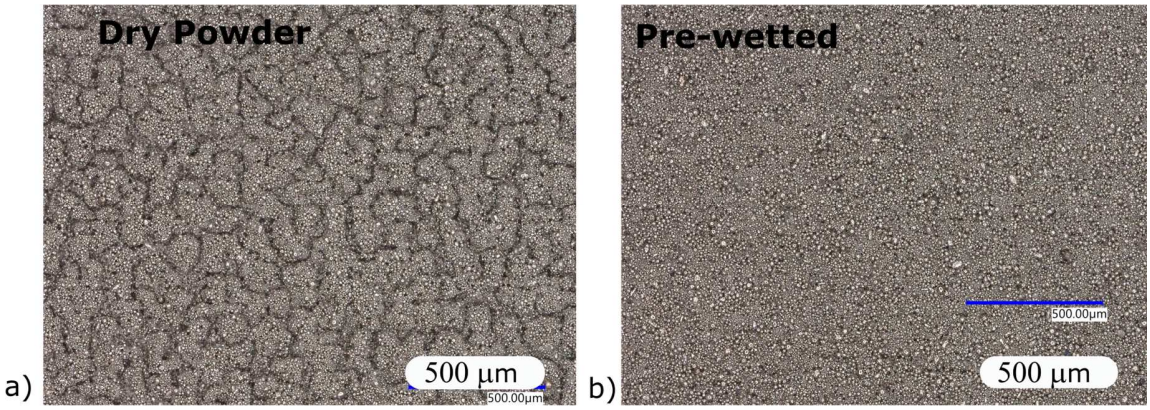

Figure 15: Images of the first printed layer on (a) dry powdered and (b) powder that was prewetted with 0.016 mg/cm^2 of prewetting moisture. Both lines were printed with 50 µm droplet and line spacing, 5 m/s droplet velocity, and 1000 Hz frequency.

Figure 14 shows that the dry powder increased in roughness during printing similar to prior work [20]. Prewetting the powder bed virtually eliminates increase in Sa values due to printing, and in some cases, prewetting even reduces Sa values below that of the undisturbed powder bed. If part defects are caused by these increased Sa values, prewetting would likely eliminate them. The images of the printed layers in Figure 15 visually illustrate the difference in Sa between dry and prewetted layers. The layer printed in dry powder shows signs of a balling like phenomena which is largely mitigated in the layer printed into prewetted powder.

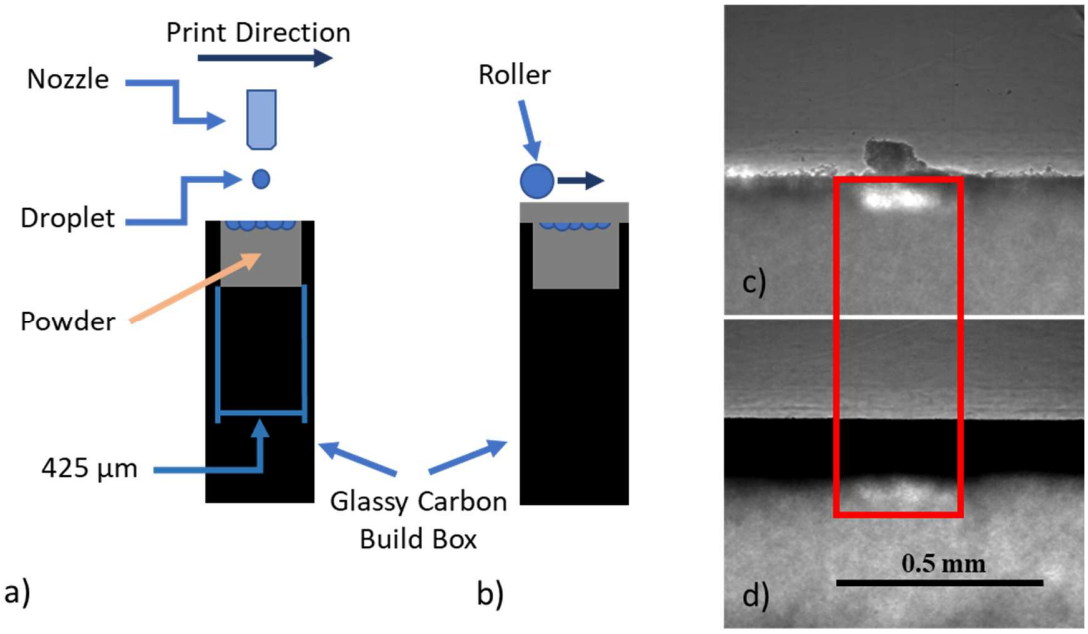

Figure 16: a) Experimental setup for corresponding X-ray images (c) viewed looking down the axis of the line. A defect (bright region) is created. These tests were conducted in non-rolled powder. Images on the left show the printing conditions for the x-ray images on the right where a clear area of lower density can be seen just under the surface of the powder bed. c) a line printed forming a defect. d) the same line from (a) with a fresh layer rolled on top. The dark region is the wider layer on top of the build box that the x-ray cannot penetrate. After rolling a layer of powder over the top, the defect persists. (Outlined in red). X-ray framerate was ~50000 frames per second with an exposure time of 19 µs.

X-ray imaging conducted at APS also provided a visual representation of possible void formation during the printing process. These conditions do not fully reproduce printing parameters, but they provide evidence of the defect persistence after spreading a new layer of powder. Figure 16 shows a layer (5 lines) printed into dry powder along the axis of the X-ray beam so that the line cross section is clearly visible. A region of much lower density can be seen just under the surface of the powder where printing reduced the powder bed density. A layer of new powder was spread over the build box and the entire printed region. After spreading, the low-density region still persists below the spread layer (Figure 16d). Although the initial powder layer was spread with a blade rather than a roller, this shows that a low-density region can persist after layer spreading. Such low-density regions could persist in the final part and may be a source of the pores seen in BJ parts after sintering.

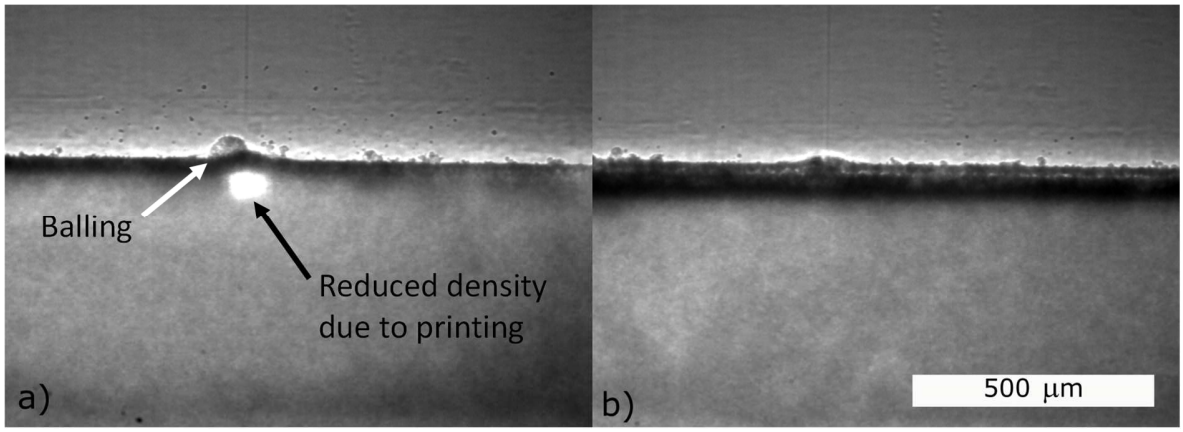

Figure 17: X-ray images comparing line formation in dry and prewetted powder. Lines were printed parallel to the x-ray beam as illustrated in Figure 16. Left: This layer was printed into a dry powder bed. A clear area of less density can be seen just under the surface of the powder bed. The lower-density area could be the creation of a void within the powder bed. Right: This layer was printed into a prewetted powder bed. The less-dense area seen in the dry powder is absent from the prewetted bed. These tests were conducted in non-rolled powder. X-ray framerate was ~50000 frames per second with an exposure time of 19 µs.

In Figure 17a, the density decreases from printing a line into dry powder is clearly visible. However, when printed into prewetted (0.0164 mg/cm^2) powder (Figure 17b), no density change is observed from printing. The prewetting process not only mitigates balling, particle rearrangement, and particle ejection, but also eliminates low density regions that may be forming during the printing process.

4 CONCLUSIONS

This paper assesses the effects of prewetting a powder bed on the formation of 1D (lines), 2D (single layers), and 3D (multi-layers) printed geometry. This provides insights into the potential impact of prewetting the powder on part accuracy, strength, and quality. This work showed that tri-ethylene glycol can be successfully used to prewet a powder bed prior to printing in BJ AM. Once applied, a repeatable fraction of the tri-ethylene remains within the powder bed for the duration of the printing sequence. Prewetting and subsequent partially drying may create a non-percolating prewetted condition that aids binder infiltration and increases powder cohesion without causing excessive spreading of the binder.

Prewetting with this mixture significantly expands the ranges of droplet spacing that creates continuous lines and eliminates the roughness increase in the first printed layers observed in dry powders. These changes may also help reduce the formation of pores between part layers. Inspection of parts and X-ray high speed imaging of the printing process show that the prewetting reduces balling, particle ejection and powder rearrangement. Persistent defects in sintered BJ parts have been attributed to particle ejection and powder rearrangement. The ability to reduce ejection and rearrangement is likely to improve properties of sintered BJ components.

The benefits of prewetting can be maximized, and drawbacks lessened by adding small amounts of moisture. Increased prewetting moisture levels increase part dimensions. When prewetting, the binder spreads more horizontally than vertically, creating a larger aspect ratio of width/depth. This may reduce printing saturation but the effect is reduced when printing multiple layers. While prewetting reduced saturation in the lines, prewetting increases saturation levels in

layers up to 20% compared to printing into dry powder. This can increase the strength of green parts to allow finer features and reduce damage in handling. This may be related to differences in drying time between the layers for dry and prewetted powder, but it demonstrates that with drying, high levels of saturation can be achieved in multi-layer parts printed in prewetted powder. In production, this could be accomplished quickly with powder bed heating. The results were not significantly impacted by changes in droplet velocity or printing frequency over the range studied.

These results suggest that prewetting the powder may be very effective in improving the quality of printed BJ parts. Additional work is needed to test these impacts over a broader range of print parameters and larger geometries and to see whether predictive tools from other areas such as granulation [42, 43] provide insight into BJ printing. Additionally, it will be helpful to quantify the impacts of prewetting on sintered parts and to assess the impact of drying between layers [2] (as is typically practiced in industry).

ACKNOWLEDGEMENTS

This material is based upon work supported by the National Science Foundation through award CMMI-19467 and the NRC through award 31310019M0006. This research used resources at the Advanced Photon Source, a US Department of Energy (DOE) Office of Science User Facility operated for the DOE Office of Science by Argonne National Laboratory under Contract No. DE-AC02-06CH11357.

REFERENCES

[1] M. Ziaee, and N. B. Crane, “Binder jetting: A review of process, materials, and methods,” *Additive Manufacturing,* vol. 28, pp. 781-801, 2019.

[2] N. B. Crane, “Impact of part thickness and drying conditions on saturation limits in binder jet additive manufacturing,” *Additive Manufacturing,* vol. 33, 2020.

[3] X. Lv, F. Ye, L. Cheng, S. Fan, and Y. Liu, “Binder jetting of ceramics: Powders, binders, printing parameters, equipment, and post-treatment,” *Ceramics International,* vol. 45, no. 10, pp. 12609-12624, 2019.

[4] M. Li, W. Du, A. Elwany, Z. Pei, and C. Ma, “Metal Binder Jetting Additive Manufacturing: A Literature Review,” *Journal of Manufacturing Science and Engineering,* vol. 142, no. 9, pp. 1-45, 2020-09-01, 2020.

[5] P. Nanthananon, S. Tanodekaew, P. Tesavibul, S. Manotham, P. Kaewkong, and S. Channasanon, “Enhancing the mechanical properties of photosensitive binder jetting PLA via dual curing and thermal treatment,” *Journal of Applied Polymer Science,* vol. 139, no. 15, 2022.

[6] W. Du, X. Ren, C. Ma, and Z. Pei, "Binder jetting additive manufacturing of ceramics: A literature review," *ASME International Mechanical Engineering Congress and Exposition, Proceedings (IMECE).* p. ASME.

[7] M. Zago, N. F. M. Lecis, M. Vedani, and I. Cristofolini, “Dimensional and geometrical precision of parts produced by binder jetting process as affected by the anisotropic shrinkage on sintering,” *Additive Manufacturing,* vol. 43, 2021.

[8] S. Sadeghi Borujeni, A. Shad, K. Abburi Venkata, N. Gunther, and V. Ploshikhin, “Numerical simulation of shrinkage and deformation during sintering in metal binder jetting with experimental validation,” *Materials and Design,* vol. 216, 2022.

[9] N. Lecis, R. Beltrami, and M. Mariani, “Binder jetting 3D printing of 316 stainless steel: Influence of process parameters on microstructural and mechanical properties,” *Metallurgia Italiana,* vol. 113, no. 2, pp. 31-41, 2021.

[10] M. Mariani, R. Beltrami, F. Meneghetti, D. Azzollini, and N. Lecis, "Effect of Printing Parameters on the Mechanical Strength of Green Body from Binder Jetting Additive Manufacturing," *Proceedings - Euro PM2020 Congress and Exhibition*.

[11] Y. Bai, C. Wall, H. Pham, A. Esker, and C. B. Williams, “Characterizing Binder–Powder Interaction in Binder Jetting Additive Manufacturing Via Sessile Drop Goniometry,” *Journal of Manufacturing Science and Engineering,* vol. 141, no. 1, 2019.

[12] S. Barui, H. Ding, Z. Wang, H. Zhao, S. Marathe, W. Mirihanage, B. Basu, and B. Derby, “Probing Ink-Powder Interactions during 3D Binder Jet Printing Using Time-Resolved X-ray Imaging,” *ACS Applied Materials and Interfaces,* vol. 12, no. 30, pp. 34254-34264, 2020.

[13] H. Miyanaji, S. Zhang, and L. Yang, “A new physics-based model for equilibrium saturation determination in binder jetting additive manufacturing process,” *International Journal of Machine Tools and Manufacture,* vol. 124, pp. 1-11, 2018.

[14] V. Sufiiarov, A. Kantyukov, A. Popovich, and A. Sotov, “Structure and properties of barium titanate lead-free piezoceramic manufactured by binder jetting process,” *Materials,* vol. 14, no. 16, 2021.

[15] D. A. Schlachter, M. D. Lennox, B. D. Favis, D. Therriault, and J. R. Tavares, “Physicochemical Limitations of Capillary Models Applied to High-Concentration Polymer Solutions,” *ACS Omega,* vol. 7, no. 7, pp. 5636-5645, 2022-02-22, 2022.

[16] H. Tan, “Three-dimensional simulation of micrometer-sized droplet impact and penetration into the powder bed,” *Chemical Engineering Science,* vol. 153, pp. 93-107, 2016.

[17] J. J. Wagner, and C. Fred Higgs, III, “Computation of Hydrodynamic and Capillary Phenomena in Binder Jet Three-Dimensional Printing,” *Journal of Tribology,* vol. 143, no. 5, 2021.

[18] S. L. Fuchs, P. M. Praegla, C. J. Cyron, W. A. Wall, and C. Meier, “A versatile SPH modeling framework for coupled microfluid-powder dynamics in additive manufacturing: binder jetting, material jetting, directed energy deposition and powder bed fusion,” *Engineering with Computers,* vol. 38, no. 6, pp. 4853-4877, 2022/12/01, 2022.

[19] T. Colton, and N. B. Crane, “Influence of droplet velocity, spacing, and inter-arrival time on line formation and saturation in binder jet additive manufacturing,” *Additive Manufacturing,* vol. 37, 2021.

[20] T. Colton, C. Inkley, A. Berry, and N. B. Crane, “Impact of inkjet printing parameters and environmental conditions on formation of 2D and 3D binder jetting geometries,” *Journal of Manufacturing Processes,* vol. 71, pp. 187-196, 2021/11/01/, 2021.

[21] T. Colton, J. Liechty, A. McLean, and N. Crane, "Influence of drop velocity and droplet spacing on the equilibrium saturation level in binder jetting," *Solid Freeform Fabrication 2019: Proceedings of the 30th Annual International Solid Freeform Fabrication Symposium - An Additive Manufacturing Conference, SFF 2019.* pp. 99-108.

[22] C. Inkley, D. Martin, B. Clark, and N. Crane, “Controlled Wetting of Spread Powder and its Impact On Line Formation in Binder Jetting,” in Manufacturing Science and Engineering Conference (MSEC2022), West Lafayette, Indiana, USA, 2022.

[23] Y. Bai, G. Wagner, and C. B. Williams, “Effect of Particle Size Distribution on Powder Packing and Sintering in Binder Jetting Additive Manufacturing of Metals,” *Journal of Manufacturing Science and Engineering,* vol. 139, no. 8, 2017.
[24] M. Ziaee, E. M. Tridas, and N. B. Crane, “Binder-Jet Printing of Fine Stainless Steel Powder with Varied Final Density,” *Jom,* vol. 69, no. 3, pp. 592-596, 2016.
[25] P. Kumar, and K. S. R. Chandran, “StrengthDuctility Property Maps of Powder Metallurgy (PM) Ti-6Al-4V Alloy: A Critical Review of Processing-Structure-Property Relationships,” *Metallurgical and Materials Transactions A: Physical Metallurgy and Materials Science,* vol. 48, no. 5, pp. 2301-2319, 2017.
[26] P. Petrovskiy, M. Khomutov, V. Cheverikin, A. Travyanov, A. Sova, and I. Smurov, “Influence of hot isostatic pressing on the properties of 316L stainless steel, Al-Mg-Sc-Zr alloy, titanium and Ti6Al4V cold spray deposits,” *Surface and Coatings Technology,* vol. 405, 2021.
[27] A. Yegyan Kumar, J. Wang, Y. Bai, S. T. Huxtable, and C. B. Williams, “Impacts of process-induced porosity on material properties of copper made by binder jetting additive manufacturing,” *Materials and Design,* vol. 182, 2019.
[28] T. Do, T. J. Bauder, H. Suen, K. Rego, J. Yeom, and P. Kwon, "Additively manufactured full-density stainless steel 316L with binder jet printing," *ASME 2018 13th International Manufacturing Science and Engineering Conference, MSEC 2018.* p. Manufacturing Engineering Division.
[29] T. Do, P. Kwon, and C. S. Shin, “Process development toward full-density stainless steel parts with binder jetting printing,” *International Journal of Machine Tools and Manufacture,* vol. 121, pp. 50-60, 2017.
[30] P. Nandwana, A. M. Elliott, D. Siddel, A. Merriman, W. H. Peter, and S. S. Babu, “Powder bed binder jet 3D printing of Inconel 718: Densification, microstructural evolution and challenges,” *Current Opinion in Solid State & Materials Science,* vol. 21, no. 4, pp. 207-18, 08/, 2017.
[31] A. Mostafaei, P. Rodriguez De Vecchis, E. L. Stevens, and M. Chmielus, “Sintering regimes and resulting microstructure and properties of binder jet 3D printed Ni-Mn-Ga magnetic shape memory alloys,” *Acta Materialia,* vol. 154, pp. 355-364, 2018.
[32] C. Zheng, A. Mostafaei, P. R. de Vecchis, I. Nettleship, and M. Chmielus, “Microstructure evolution for isothermal sintering of binder jet 3D printed alloy 625 above and below the solidus temperature,” *Additive Manufacturing,* vol. 47, 2021.
[33] A. Mostafaei, P. Rodriguez De Vecchis, I. Nettleship, and M. Chmielus, “Effect of powder size distribution on densification and microstructural evolution of binder-jet 3D-printed alloy 625,” *Materials and Design,* vol. 162, pp. 375-383, 2019.
[34] E. Stevens, S. Schloder, E. Bono, D. Schmidt, and M. Chmielus, “Density variation in binder jetting 3D-printed and sintered Ti-6Al-4V,” *Additive Manufacturing,* vol. 22, pp. 746-752, 2018-08-01, 2018.
[35] Y. Bai, G. Wagner, and C. B. Williams, “Effect of particle size distribution on powder packing and sintering in binder jetting additive manufacturing of metals,” *Journal of Manufacturing Science and Engineering, Transactions of the ASME,* vol. 139, no. 8, 2017.
[36] N. D. Parab, J. E. Barnes, C. Zhao, R. W. Cunningham, K. Fezzaa, A. D. Rollett, and T. Sun, “Real time observation of binder jetting printing process using high-speed X-ray imaging,” *Scientific Reports,* vol. 9, no. 1, pp. 2499, 2019/02/21, 2019.

[37] K. M. Rahman, A. Wei, H. Miyanaji, and C. B. Williams, “Impact of binder on part densification: Enhancing binder jetting part properties through the fabrication of shelled geometries,” *Additive Manufacturing,* vol. 62, pp. 103377, 2023/01/25/, 2023.
[38] T. Fan, “Droplet-powder impact interaction in three dimensional printing,” Mechanical Engineering, Massachussetts Institute of Technology, Cambridge, MA, 1996.
[39] H. Tan, “Absorption of millimeter- and micrometer-sized droplets on nylon powder,” *Experiments in Fluids,* vol. 63, no. 12, 2022-12-01, 2022.
[40] R. K. Holman, M. J. Cima, S. A. Uhland, and E. Sachs, “Spreading and Infiltration of Inkjet-Printed Polymer Solution Droplets on a Porous Substrate,” *Journal of colloid and interface science,* vol. 249, no. 2, pp. 432-440, 2002.
[41] H. N. Emady, D. Kayrak-Talay, and J. D. Litster, “Modeling the granule formation mechanism from single drop impact on a powder bed,” *Journal of colloid and interface science,* vol. 393, no. 1, pp. 369-376, 2013.
[42] H. N. Emady, D. Kayrak-Talay, and J. D. Litster, “A regime map for granule formation by drop impact on powder beds,” *AIChE Journal,* vol. 59, no. 1, pp. 96-107, 2013.
[43] H. N. Emady, D. Kayrak-Talay, W. C. Schwerin, and J. D. Litster, “Granule formation mechanisms and morphology from single drop impact on powder beds,” *Powder Technology,* vol. 212, no. 1, pp. 69-79, 2011.
[44] N. Eshtiaghi, and K. P. Hapgood, “A quantitative framework for the formation of liquid marbles and hollow granules from hydrophobic powders,” *Powder Technology,* vol. 223, pp. 65-76, 2012.
[45] K. P. Hapgood, T. H. Nguyen, S. Hauw, S. M. Iveson, and W. Shen, “Rewetting Effects and Droplet Motion on Partially Wetted Powder Surfaces,” *AIChE Journal,* vol. 55, no. 6, pp. 1402-1415, 2009.
[46] T. Nguyen, W. Shen, and K. Hapgood, “Drop penetration time in heterogeneous powder beds,” *Chemical Engineering Science,* vol. 64, no. 24, pp. 5210-5221, 2009/12/16/, 2009.
[47] K. P. Hapgood, J. D. Litster, S. R. Biggs, and T. Howes, “Drop Penetration into Porous Powder Beds,” *Journal of Colloid and Interface Science,* vol. 253, no. 2, pp. 353-366, 2002/09/15/, 2002.
[48] H. Chen, and Y. F. Zhao, “Process parameters optimization for improving surface quality and manufacturing accuracy of binder jetting additive manufacturing process,” *Rapid Prototyping Journal,* vol. 22, no. 3, pp. 527-538, 2016.
[49] M. Lanzetta, and E. Sachs, “Improved surface finish in 3D printing using bimodal powder distribution,” *Rapid Prototyping Journal,* vol. 9, no. 3, pp. 157-166, 2003.
[50] T. Colton, “The Impact of Inkjet Parameters and Environmental Conditions in Binder Jetting Additive Manufacturing,” Mechanical Engineering, Brigham Young University, 2020.
[51] T. Fan, “Droplet-Powder Impact Interaction In Three Dimensional Printing,” Massachusetts Institute Of Technology, 1995.
[52] J. R. Nimmo, "Vadose Water," *Encyclopedia of Inland Waters*, G. E. Likens, ed., pp. 766-777, Oxford: Academic Press, 2009.
[53] Y. Mualem, “A new model for predicting the hydraulic conductivity of unsaturated porous media,” *Water Resources Research,* vol. 12, no. 3, pp. 513-522, 1976.
[54] T. O. Althaus, and E. J. Windhab, “Characterization of wet powder flowability by shear cell measurements and compaction curves,” *Powder Technology,* vol. 215-216, pp. 59-65, 2012.

[55] L. Marchetti, P. Mellin, and C. Neil Hulme, “Negative impact of humidity on the flowability of steel powders,” *Particulate Science and Technology*, pp. 1-15, 2021-11-25, 2021.
[56] H. Chen, "A Process Modelling and Parameters Optimization and Recommendation System for Binder Jetting Additive Manufacturing Process."
[57] R. K. Enneti, and K. C. Prough, “Effect of binder saturation and powder layer thickness on the green strength of the binder jet 3D printing (BJ3DP) WC-12%Co powders,” *International Journal of Refractory Metals and Hard Materials,* vol. 84, 2019.
[58] R. Jiang, L. Monteil, K. Kimes, A. Mostafaei, and M. Chmielus, “Influence of powder type and binder saturation on binder jet 3Dprinted and sintered Inconel 625 samples,” *International Journal of Advanced Manufacturing Technology,* vol. 116, no. 11-12, pp. 3827-3838, 2021.
[59] J. Ruprecht, K. Agarwal, and S. Ahmed, "Binder saturation, layer thickness, drying time and their effects on dimensional tolerance and density of cobalt chrome - tricalcium phosphate biocomposite," *Solid Freeform Fabrication 2019: Proceedings of the 30th Annual International Solid Freeform Fabrication Symposium - An Additive Manufacturing Conference, SFF 2019.* pp. 148-157.
[60] J. Lawrence, H. A. Pena Vega, B. Stegman, C. Roberts, J. Spencer, C. James, M. Christensen, and N. Crane, "Construction of Open-Source Laboratory-Scale Binder Jetting System for High-Speed Synchrotron X-Ray Imaging," 2022.
[61] J. Lawrence, C. Inkley, K. Fezzaa, S. J. Clark, and B. Crane Nathan, “Observations of Binder Jetting Defect Formation Using High-Speed Synchrotron X-Ray Imaging,” in 2022 Solid Freeform Fabrication Symposium, Austin, TX, 2022.
[62] R. Lenhard, J. Parker, and S. Mishra, “COREY AND VAN GENUCHTEN MODELS,” *J. Irrig. Drain Eng,* vol. 115, no. 4, pp. 744-751, 1989.
[63] J. Hamilton, D. Daniel, and R. Olson, “Measurement of Hydraulic Conductivity of Partially Saturated,” *Permeability and groundwater contaminant transport*, no. 746, pp. 182, 1981.
[64] K. E. Fielden, J. M. Newton, and R. C. Rowe, “Movement of liquids through powder beds,” *International Journal of Pharmaceutics,* vol. 79, no. 1, pp. 47-60, 1992/02/01/, 1992.
[65] R. G. Larson, and N. R. Morrow, “Effects of sample size on capillary pressures in porous media,” *Powder Technology,* vol. 30, no. 2, pp. 123-138, 1981/11/01/, 1981.
[66] N. R. Morrow, “IRREDUCIBLE WETTING-PHASE SATURATION IN POROUS MEDIA,” *Chemical Engineering Science,* vol. 25, no. 11, pp. 1799-1815, 1970.

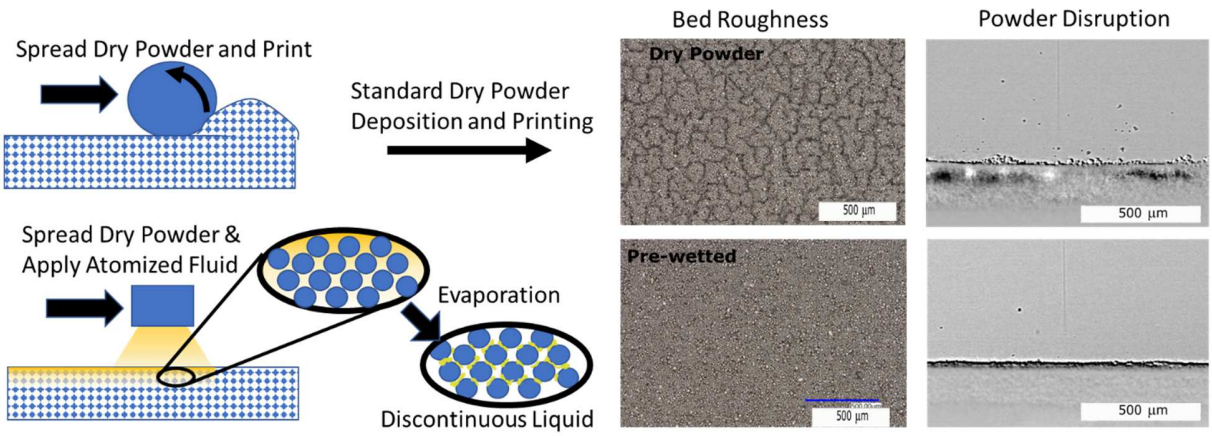
Spread Dry Powder and Print
Standard Dry Powder
Deposition and Printing
Spread Dry Powder &
Apply Atomized Fluid
Evaporation
Discontinuous Liquid
Bed Roughness
Powder Disruption
Dry Powder
Pre-wetted
500 µm
500 µm
500 µm
500 µm